Journal of Petroleum Science and Engineering 151 (2017) 169–182

Contents lists available at ScienceDirect

Journal of Petroleum Science and Engineering

journal homepage: www.elsevier.com/locate/petrol

A new method for rock brittleness evaluation in tight oil formation from conventional logs and petrophysical data

Xian Shi[a], Jian Wang[b,*], Xinmin Ge[c], Zhongying Han[d], Guanzheng Qu[e], Shu Jiang[f]

[a] Unconventional Oil & Gas and Renewable Energy Research Institute, China University of Petroleum (Huadong), Qingdao, Shandong 266555, China
[b] College of Science, China University of Petroleum (Huadong), Qingdao, Shandong 266555, China
[c] College of Geoscience, China University of Petroleum (Huadong), Qingdao, Shandong 266555, China
[d] College of Petroleum Engineering, China University of Petroleum (Huadong), Qingdao, Shandong 266555, China
[e] College of Petroleum Engineering, Xi'an Shiyou University, Xi'an, Shanxi 710065, China
[f] Energy & Geoscience Institute, University of Utah, Salt Lake City, UT 84108, USA

ARTICLE INFO

Keywords:
Rock brittleness
Computational intelligence
Tight oil
Multilayer perception
Radial basis function
Hydraulic fracturing

ABSTRACT

Brittleness is a critical indicator for hydraulic fracturing candidate screening in unconventional reservoirs. Current rock brittleness estimation models are often inferred from mechanical parameters and mineralogical data, which primarily use empirical equations. However, the absence of shear sonic velocity data and insufficient mineral data sometimes restricts its wide application. In this article, our objective is to illustrate the application of a data-driven approach for rock brittleness estimation that employs computational intelligence technologies (multilayer perception and radial basis function models) that use conventional well logs as inputs. To reflect the local rock type variation with depth, we first updated the typical mineralogy based brittleness calculation formulas. A database of the well logs, mechanical parameters, X-ray diffraction (XRD) and QEMSCAN mineralogy results collected from a single well in the Santanghu tight oil formation in the Xinjiang basin, China was then constructed. Rock brittleness tests were performed using a multilayer perception model and radial basis function model with different inputs. The comparison of the rock brittleness results produced by the log-based soft computing technologies, mechanical-based method and mineralogy-based method demonstrated that the data-driven approach is flexible and has sufficient accuracy. According to the performance indicators, the predictive performance of the radial basis function model was found to be better than that of the multilayer perception model. This study shows that soft computing technologies can be used to infer missing data when the mineralogical data are inadequate and are less dependent on acoustic full-wave logging, and they are therefore more applicable and practical than traditional empirical formulas.

1. Introduction

Unconventional reservoirs are becoming a significant contributor to hydrocarbon production across the world. Because the gas flow resistance of unconventional reservoirs is much greater than that of conventional reservoirs, the combination of horizontal drilling and multistage hydraulic fracturing technology is commonly used to enhance hydrocarbon production by creating efficient complex fracture networks (Cipolla et al., 2008; Chong et al., 2010). Previous reports have shown that the successful creation of a complex fracture network is related to increased rock brittleness. Therefore, rock brittleness is usually regarded as an important mechanical parameter when describing formations that are likely to generate complex fracture networks under hydraulic fracturing. Although researchers have performed many studies on brittleness, there is still no universal definition and applicable standard for brittleness evaluation because of different physical sources. Rock brittleness can be calculated using stress-stain curves obtained from triaxial measurements, including the ratio of the elastic strain and total strain, the ratio of the compressive to tensile strengths, friction angle, Brinell hardness, axial point load, and empirical equations that involve stress and strain (Hucka et al., 1974; Altindag et al., 2004; Li et al., 2013; Heidari et al., 2014; Zhou et al., 2014; Kias et al., 2015). However, it is not feasible to evaluate rock brittleness using triaxial laboratory measurements due to the limitations of intact samples and expense. Brittleness estimates employing mineralogical analyses and well logs are more practical because the information is more easily and cheaply gathered from laboratory and downhole measurements than from mechanical tests.

* Corresponding author.
E-mail address: nikebill@163.com (J. Wang).

http://dx.doi.org/10.1016/j.petrol.2016.12.036
Received 21 February 2016; Received in revised form 22 October 2016; Accepted 27 December 2016
Available online 29 December 2016
0920-4105/

Those attempts to estimate brittleness have had a certain degree of success, but they also have drawbacks. Recently, some authors have tried to build correlations between brittleness and well logs because that data-driven approach is universally applicable and more practical than employing physical equations. Jin et al. (2014a, 2014b) studied the relationships between rock brittleness and well logs and presented a statistical regression analysis of brittleness based on porosity vs. brittleness crossplots and sonic compressional slowness vs. brittleness crossplots. The application of that novel method has enjoyed a certain success in typical U.S shale gas plays (Woodford, Barnett and Eagle ford). Wang et al. (2015) developed a brittleness model using the ratio of gamma rays to photoelectric absorption cross section index (GR/Pe), and they illustrated that brittleness variations can be observed using special well logs alterations along the wellbore because the Pe log can be used to discriminate different brittle minerals. However, because the study area is in the Chang 7 shaly sandstone in the Ordos Basin in China, more studies are needed to validate whether this empirical correlation is only applicable in this basin. In addition, Pe logs are not always available for all wells, which therefore also restricts its wide application.

Because there are complex relationships between brittleness and non-linear and fuzzy well log data, traditional simple regression and multiple-regression methods cannot guarantee enough accuracy, even if those methods are usually easy to apply. Furthermore, in most cases, one major drawback of single-log brittleness estimation is the assumption that no large variations in other parameters exist that can affect the reading of the logs; however, this type of approach heavily depends on independent well logging quality, and, otherwise, substantial errors potentially exist. To offset some of these problems, prediction technologies, such as artificial neural networks, can be utilized for the prediction of rock brittleness. Neural networks are capable of dealing with complicated and unknown multilinear problems, and they are characterized as computational models with particular abilities to adapt, learn, generalize, recognize, cluster and organize data (Huang et al., 2003). In recent years, artificial neural networks have been successfully employed for developing predictive models in many petroleum fields such as sand control, permeability and porosity prediction, drilling optimization, EOR candidate and fracturing candidate optimization (Parada et al., 2012; Obersinkler et al., 2003). The data-driven based features of this modeling approach can provide increased flexibility for self-adjustment to adapt to various ranges of data. As a matter of fact, the prediction of rock brittleness is of a similar nature, but artificial intelligence technologies have not yet been used for rock brittleness in hydrocarbon plays.

The purpose of this study is to outline a data-based approach for brittleness estimation using multi-layer perception (MLP) and radial basis function (RBF) models. Because the quality of the inputs of the computational intelligence models discussed below is critical, establishing a reliable brittleness dataset is the primary step. An initial effort has been made in this study to establish a brittleness dataset for a tight oil formation in the Xinjiang Basin, China, using mineralogical XRD and QEMSCAN analyses. Additional work was performed to assess the possible connections between the material properties and brittleness in terms of the mineralogical contents and elastic parameters from well logs, and therefore more appropriate brittleness calculations can be selected. The development of the new prediction models is discussed in detail, and the outputs of the models are also discussed in this paper. The results from the MLP and RBF models are compared to reveal the efficiency of the prediction processes of the two networks.

2. Materials and methods

2.1. study area

Well H is a pilot well in the Permian Lucaogou Formation of the Santanghu Basin in China. The Santanghu Basin is situated in the Hami area in the NE Xinjiang Uyghur Autonomous Region. It is an NW–SE striking basin that covers an area of 2.3×10^4 km^2. It can be divided into three first-order tectonic units: a northern uplift belt, center depression belt and southern thrust nappe belt. The center depression can be further subdivided into five highs and six sags. The Malang-Tiaohu Sags, which has an area of 3200 km^2, is the primary area for oil and gas exploration and development. The advantages of the Santanghu tight oil are its large thickness (100–300 m), wide distribution and good preservation. In recent years, exploration and production tasks within the Santanghu formation have been performed by PetroChina, and commercial tight oil has been obtained. The promising tight oil prospects in this area are indicated by some appraisal wells. The reservoir has characteristically high brittleness, high oil saturation and high-density oil. The oil in the 2nd member of the Tiaohu Formation is sourced from the Lucaogou high quality source rock underneath. The main migration pathway is faults, and the migration distances range from 100 m to 500 m. The unique tuffite (tuff limestone, pyroclastic and detrital sandstone) reservoir is different from shale, sandstone, and carbonate reservoirs. The accumulation of tight oil in the tuffite is mainly controlled by the distribution and properties of the Lucaogou source rock and tuffite reservoir within the 2nd member of the Tiaohu Formation.

The structures in this study area consist of gentle anticlines showing a north-south general trend. Prior reservoir characterization results show that the TOC content of the hydrocarbon rocks ranges from 0.01% to 18.79%, and the kerogen of the organic matter is predominantly of Types III and II2. The target sedimentary tuffite formations are characterized by porosity of 16.2–21.7%, permeability of 0.0001×10^{-3}–0.500×10^{-3} μm^2, a stable areal distribution of the matrix pore volumes and their constituents, a large variation in the fracture and pore characteristics among the different tectonic regions as well as the different well fields and different intervals in the same tectonic. According to previous studies, the tuffite in the Permian Tiaohu Formation is a fine-grained tight reservoir with high porosity and low permeability. The pore throats are dominated by 88.3% nano-scale pore throats, and the air permeability is less than 0.5×10^{-3} μm^2. Because most rock samples have low porosity and super-low permeability, hydraulic fracturing stimulation is necessary for commercial production.

2.2. Overview of current brittleness calculation

Typically, rock brittleness can be defined when fractures terminate at or only slightly beyond the yield stress. Hucka and Das (1974) once summarized brittleness indices proposed in different fields using laboratory measured mechanical properties. Vahid and Peter (2003) developed a plastic strain-based brittleness index (B_6) by considering cohesion weakening and friction strengthening based on the mechanism of the brittle failure of rocks. Altindag and Kahramana (2004) defined the brittleness as 50% of the product of the compressive strength and splitting tensile strength of rocks (B_2). Recent studies also reflect that rock behavior information before and after peak strength can provide additional insights into the estimation of brittleness, but the post yield and post failure behaviors of rock are hard to obtain because full cores are sometimes not available (Wang and Gale, 2009). Zhou et al. (2014) put forward new indexes for evaluating brittleness by considering the influences of the yield characteristics and stress states of rock plasticity based on the relative size and absolute value of the stress drop for postpeak strain–stress. Yang et al. (2013) investigated the relationships between brittleness and elastic and strength properties, but unfortunately, no evident correlation was found across all rock types. More authors have tried to explain the general relationship between mechanical-based brittleness and experimental data, but no evidence has been found between brittleness and single elastic parameters. One possible reason is that test results have a high degree of uncertainty when samples are brought to the surface. Mineral content

testing is an available tool to obtain relatively reliable brittleness interpretation results. However, the discrepancies in the brittleness model and brittle materials selection possibly result in erroneous interpretation results, which also demonstrates that the standards of the mineralogical method are not uniform. Given the expensive and time-consuming characteristics of core testing, this measurement remains necessary after drilling wells. Alternatively, the application of petrophysical properties for brittleness calculations that use Young's modulus and Poisson's ratio is more attractive because elastic properties can be evaluated by well logs instead of core testing (Rickman et al., 2008). Furthermore, rock brittleness can be calculated by dipole acoustic and bulk density logs simply and easily, so this method is efficient in providing a continuous estimation of rock brittleness, which is more helpful for practical guidance. Various equations have been presented to correlate the mechanical properties of rocks with their shear and compressional wave velocities. However, the Poisson's ratio and Young's modulus calculations need be computed using high-quality empirical equations if shear velocities are not available. Certainly, with the development of mineralogical logging technology, we can also obtain brittleness directly through real-time mineral components analysis, but logging service cost is a concern. Table 1 provides an overview of the current brittleness models. We can make the following conclusions.

(1) There are no universal standards for brittleness identification, and a universally applicable brittleness calculation model is virtually non-existent.
(2) Rock brittleness is not only influenced by mineral composition but is also controlled by many factors such as strain rate, temperature, pore pressure, saturation, and stress state, but it is hard to establish a model that can consider all of the affecting factors, for example, the impact of the natural fracture system on rock brittleness is difficult to be calculated by a mathematical equation.
(3) Most brittleness estimation methods are model-driven approaches, thus discrepancies exist if different parameters are involved from different physical information sources.
(4) Brittleness described using different brittleness indices can vary considerably, even when the same mechanical test data are used, and the different brittleness indices may not correlate well with rock strength or elastic properties.
(5) The well-log-based method is more applicable than the other methods, but it is a mathematical combination of elastic properties rather than a reflection of the intrinsic rock properties.

2.2.1. Mineralogical brittleness

Sondergeld et al. (2010) employed silicate mineral ratios to determine the rock brittleness index by XRD mineralogical composition. Thus, clay minerals are ductile materials because clay has extremely low frictional coefficients, and the mixing of clays can reduce the friction of a geological material. Jarvie et al. (2007) showed that there is an obvious positive correlation between brittle minerals (only quartz is considered to be a brittle rock) and brittleness. Some authors (Matthews et al., 2007; Rogers et al., 2011; Juan et al., 2012;) consider that carbonate is more brittle than clay, quartz and the other minerals, so carbonate minerals (calcite and dolomite) should be brittle minerals. Jin et al. (2014a, 2014b) adopted the proportion of brittle minerals, including quartz, feldspar and dolomite, to calculate brittleness in some shales. The brittleness calculation formulas are summarized in Table 1.

2.2.2. Elastic based brittleness

The concept of elastic-based brittleness was proposed by Rickman. The ability of a rock to fail under pressure can be described using Poisson's ratio, and the ability to continue to fracture after fracturing can be justified by Young's modulus. The formula for elastic-based rock brittleness in terms of the dynamic Young's modulus and Poisson's ratio is

$$B_7 = \frac{E_n + v_n}{2}. \tag{1}$$

The original data series must first be normalized, scaled and polarized into a comparable sequence because the dimensions of Young's modulus and Poisson's ratio are inconsistent. A min-max normalization pre-processing method is proposed prior to the rock brittleness calculation:

$$E_n = \frac{E_d - E_{\min}}{E_{\max} - E_{\min}} \tag{2}$$

$$v_n = \frac{v_{\max} - v_d}{v_{\max} - v_{\min}} \tag{3}$$

where $E_{\max}$ and $E_{\min}$ are the minimum and maximum dynamic Young's moduli, and $v_{\max}$ and $v_{\min}$ are the minimum and maximum Poisson's ratios. E_n and v_n are the normalized Young's moduli and Poisson's ratios along the depth.

Only 24 intact cores were collected successfully from this tight oil

Table 1
Brittleness calculation based on rock mineralogical compositions.

Formula	Variable declaration	References
$B_1 = \frac{W_{qtz}}{W_{qtz} + W_{cal} + W_{cl}}$	W_{qtz} is the weight of quartz, W_{dol} is the weight of dolomite, W_{cl} is the weight of clay, W_{cal} is the weight of calcite, W_{pla} is the weight of plagioclase, W_{sid} is the weight of siderite, W_{fels} is the weight of feldspar, W_{QFM} is weight of quartz, feldspar, and mica; W_{Carb} is weight of carbonate minerals consisting of dolomite, calcite, and other carbonate components.	Sondergeld et al. (2010)
$B_2 = \frac{W_{QFM} + W_{dol}}{W_{Tot}}$		Jin et al. (2014a, 2014b)
$B_3 = \frac{W_{qtz} + W_{dol}}{W_{qtz} + W_{dol} + W_{cl} + W_{cc} + W_{TOC}}$		Wang and Gale (2009) Slatt et al. (2011)
$B_4 = \frac{W_{qtz} + W_{car}}{W_{qtz} + W_{car} + W_{cl} + +W_{fels}}$		Jarvie et al. (2007) Glorioso et al. (2012)
$B_5 = \frac{W_{qtz} + W_{car} + W_{fels}}{W_{qtz} + W_{car} + W_{fels} + W_{cl}}$		Lai et al. (2016)
$B_6 = \frac{W_{qtz} + W_{dol} + W_{cal} + W_{fels} + W_{pla}}{W_{qtz} + W_{dol} + W_{cal} + W_{fels} + W_{pla} + W_{cl} + W_{sid}}$		Kias et al. (2015)
$B_7 = \sigma_c/\sigma_t$	σ_c and σ_t are compressive and tensile strength;	Altindag (2003)
$B_8 = (\sigma_c - \sigma_t)/(\sigma_c + \sigma_t)$		
$B_9 = (\tau_p - \tau_r)/\tau_p$	τ_p is peak shear strength and τ_r is residual shear strain;	Hajiabdolmajid and Kaiser (2003)
$B_{10} = (H_m - H)/K$	H and H_m are macro and micro-hardness, K is bulk modulus	Honda and Sanada (1956)
$B_{11} = \varepsilon_r/\varepsilon_t$	ε_r and ε_t are recoverable and total strains	Hucka and Das (1974)
$B_{12} = \sin\varphi$	φ is internal fiction angle	Hucka and Das (1974)
$B_{13} = 45^0 + \varphi/2$		

formation, and all samples were treated according to ASTM procedures. The samples had a diameter of approximately 25 mm and a length of 50 mm. It should be noted that all of the samples were drilled in a vertical orientation relative to the bedding plane. In the laboratory, the elastic dynamic properties can be derived by acoustic measurements, which assumes that the acoustic velocities are related to the rock elastic properties. In practical use, the dynamic Young's modulus and Poisson's ratio can be determined using full-waveform sonic logs, but sometimes the lack of shear wave travel times require the establishment of local empirical equations or the other means to infer elastic properties (Mullen et al., 2007). The acoustic P-wave and S-wave signals were obtained at the same stress levels where the static elastic properties were measured. Then, the dynamic Young's modulus and Poisson's ratio can be calculated by the following equations:

$$E_d = \rho V_s^2 \frac{3V_p^2 - 43V_s^2}{V_p^2 - V_s^2} \tag{4}$$

$$\nu_d = \frac{V_p^2 - 2V_s^2}{2(V_p^2 - V_s^2)} \tag{5}$$

where ρ is the bulk density, which can be measured in the lab or from density logs. The V_P are the compressional wave velocities (m/s), and the V_s are the shear wave velocities (m/s).

3. Data analysis

3.1. 1 Experimental results

The main rock types in this study are volcanic sedimentary rocks (tuffite or tuff limestone and tuff gritstone) and tight sandstone. Their sedimentary structures are relatively stable. The intergranular pores are relatively well preserved. Secondary pores are developed and are dominated by intra-particle dissolved pores. Among the secondary fractures, tectonic fractures are predominant, followed by dissolved fractures. The fractures are partially open, as shown by SEM image (Fig. 1). QEMSCAN technology and X-ray diffraction (XRD) were used for fabric and mineralogy tests on core samples and drilling cuttings. Prior to the experiments, all of the samples were stored in inert oil for better preservation. The mineralogy test results indicated that the studied reservoir is dominated by dolomite, calcite, quartz, clay, plagioclase, feldspar and pyrite. Some samples also included dolomite, which can increase rock stiffness. Dolomite and calcite carbonate were abundant in the rock samples and ranged from 26.49% to 95.22%, with an average of 55%. The quartz content was relatively rare in some samples, and the mineral content ranged from 2.43% to 38.15% by weight. There was also the presence of pyrite, which ranged from 0% to 6.64% and averaged 4.35%. The content of clay minerals ranged from 0.39% to 12.09%. The TOC was measured by the Leco TOC method at the CNPC Key Well Logging Laboratory. The TOC values ranged from 0.15% to 5.43% and averaged 2.51%.

Only 24 intact samples were successfully obtained, and acoustic and tri-axial experiments were performed at room temperature to obtain the rock strength, elastic moduli, and acoustic velocities. In addition, these data can be used for dynamic to static elastic parameters conversions and are also beneficial for interpreting the logging-based elastic parameters. The results show that the V_p of the reservoir rock range from 4.2 to 5.8 km/s, and the V_s range from 2.8 to 3.8 km/s. The datasets used here were used to develop a useful correlation:

$$E_s = 0.1071E_d + 0.8097 \text{ and} \tag{6}$$

$$\nu_s = 0.2001\nu_d + 0.1181, \tag{7}$$

where E_S is the static Young's modulus, E_d is the dynamic Young's modulus, υ_S is the static Poisson's ratio, and υ_d is the dynamic Poisson's ratio. The dynamic Young's moduli and Poisson's ratio could then be calculated using Eqs. (4) and (5). Table 2 shows the lab test results for the Leco TOC (wt%), XRD mineralogy (wt%) and calculated elastic properties of the representative 24 intact samples.

Recent efforts indicate that the elastic-basic brittleness B_8 and mineralogical brittleness can have different magnitudes but similar shapes (Jin et al., 2014a, 2014b). Therefore, cross plots of the elastic-basic brittleness B_7 and mineralogical brittleness based on the different definitions are helpful for choosing the optimum brittle minerals to calculate the mineralogical brittleness in this basin. Although the scales of two methods are slightly different, the two variation curves are favorably consistent, and they are therefore usually jointly used to complement one another. Therefore, to offset the basin-specific differences, we adopted B_3 after the mineral content analysis of this well and presented a new brittleness by adding a statistical regression method. This method can consider the different effects of brittle mineral selection on brittleness through real weights.

$$B_8 = \frac{aW_{cal}}{bW_{TOC} + cW_{cal} + dW_{cl} + eW_{fels}}, \tag{8}$$

where a, b, c, d and e are constants obtained by least squares curve fitting using the Levenberg-Marquarat algorithm. The calculated constants are listed in Table 3. Fig. 2 shows different crossplots of the elastic-basic brittleness B_7 and mineralogical brittleness based on the different formulas. Because the weights for siderite and plagioclase are tiny for this formation, we did not calculate B_6 from the formula in Table 1. It can be observed that a strong correlation exists between B_8 and B_7, and it was concluded that the differences between the elastic-based brittleness B_7 and the values predicted by the B_8 model were less than those of the other mineralogical brittleness calculation models.

3.2. Linear modeling

Given previous reports on its relationship with porosity and compressional sonic travel time, rock brittleness can be estimated using the linear regression. To establish brittleness predictive models using the possible well logs, a linear regression analysis and coefficients were employed to estimate the brittleness. A total of 58 samples were calculated using Eq. (6) with the laboratory measurements of the mineralogical content. Out of the 58 results, approximately 75% were used in the training set, and the remaining sets were used for model testing. In this well, wireline logs were first acquired and are shown in Fig. 3; they included natural gamma ray (GR), dual laterolog (DLL, including deep laterolog, LLD, and shallow laterolog, LLS), compensated acoustic (AC), neutron porosity (CNL), lithology density (DEN), and natural spectrum logs including Uranium (U), Thorium (Th), and Potassium (K). The results obtained from the tests and the basic statistical parameters such as the average, maximum and minimum values and the standard deviations of the different parameters are given in Table 4. It should be noted that the shear velocity logging is not discussed in this paper and was only applied for the mechanical-based brittleness calculation as a comparative study because in most cases shear velocity logging is not conventionally performed.

Based on the laboratory-measured results of the core samples, the relationships between the rock brittleness and wireline logs are shown in Fig. 4. The correction coefficient (R^2) is usually a critical indicator in investigations of the influence of different well logs on laboratory-measured brittleness results. The results indicate that the rock brittleness is linearly correlated with the determination (R^2) of CNL, K, GR, DTC, and U, whereas the R^2 with LLD was poor even when using linear regression.

As shown in the figures, the CNL log vs. core brittleness had a correlation of approximately 0.69, which gave the highest correlation coefficients. However, the correlation coefficients between the different well logs were low in most cases. Fig. 4(d) shows a poor correlation of approximately 0.02645 with core brittleness vs. SP. In addition, the data from the core experiments also demonstrates that there was no direct correlation between the brittleness and GR. The low value of R^2

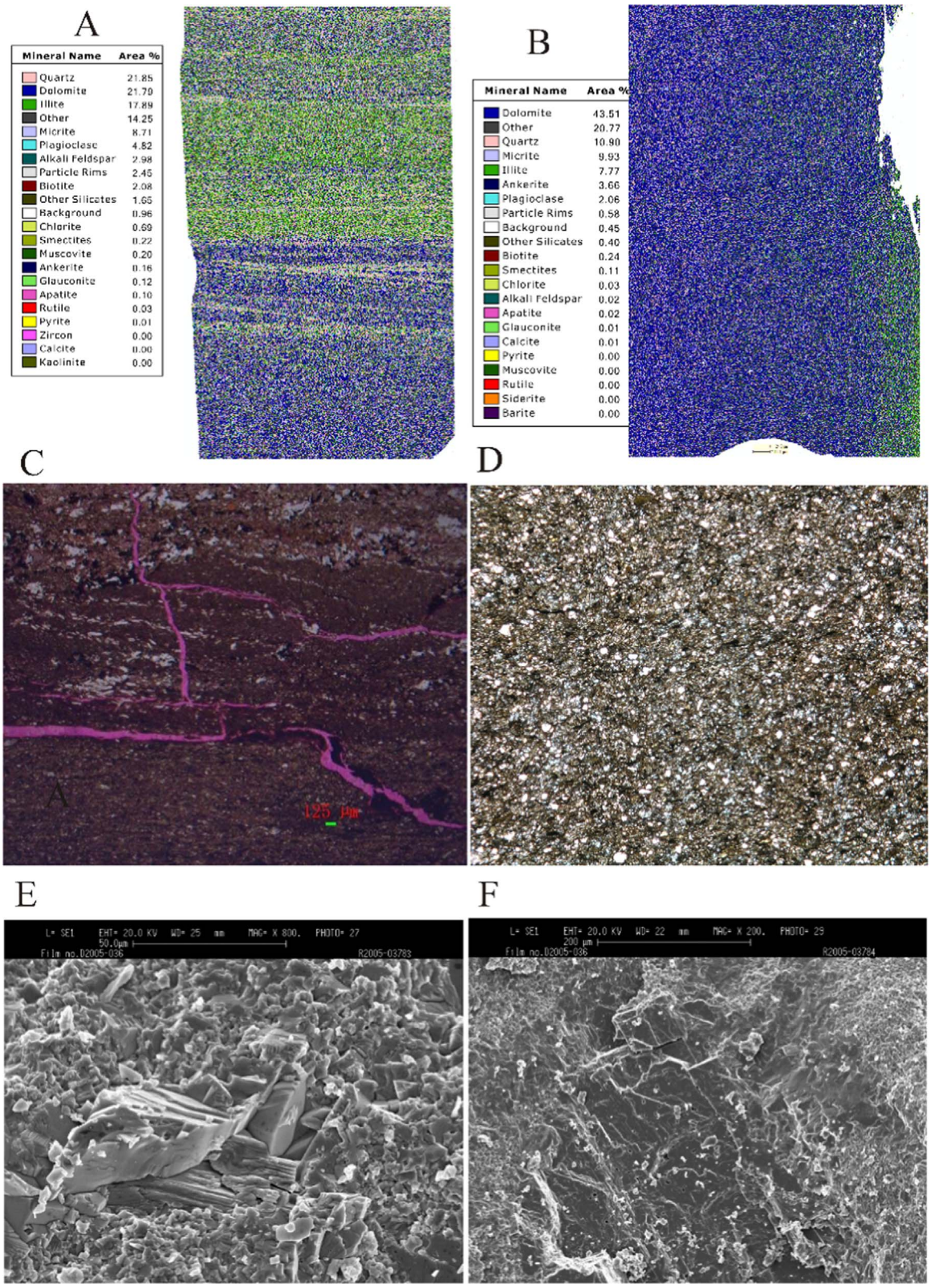

Fig. 1. QEMSCAN, SEM and Photomicrographs showing rock fabric and mineral composition for Santanghu tight tuffite formation. (A. Fine-grained, cross bedding to parallel bedding, well sorted. Mineralogy is mainly dominated by quartz, dolomite and clay. B. Mainly massive bedding, mineralogy is mainly dominated by quartz, dolomite and clay. C. Complex natural fractures filled by calcite, well H, 3072.5 m, PPL; D. Detrital quartz and feldspar rich, very fine-grained siltstone. E. Clay minerals (mainly illite and chlorite) are abundant in this sample, well H, 3125.4 m, SE. F. Clay minerals (mainly illite and chlorite), well H, 3075.1 m, SE.).

in some cases was a result of the large dispersion of the data and the remaining outlier data points, although there is an evident trend. Generally speaking, it is difficult to establish relationships between brittleness and well logs through simple regressions or nonlinear methods. To further study the correlation coefficients between of the well logs and the core measured brittleness data, a correlation

Table 2
Mineralogy determined by X-ray diffraction of target rock.

No.	TOC/%	ϕ/%	V_{cl}/%	V_{qrtz}/%	V_{fels}/%	V_{car}/%	V_{pyr}/%	E_s/GPa	v_s
1	0.33	2.66	1.36	2.43	3.30	87.80	2.13	9.06	0.16
2	0.76	1.54	5.57	6.74	14.36	64.38	6.64	8.20	0.16
3	0.35	2.15	0.78	4.29	9.17	80.93	2.34	6.75	0.18
4	0.26	0.45	0.50	2.28	1.29	95.22	0.00	8.02	0.18
5	0.40	0.91	0.39	5.03	3.06	88.53	1.68	6.82	0.18
6	1.14	2.32	7.43	6.85	13.32	65.84	3.09	4.27	0.19
7	0.30	3.01	12.09	14.50	11.70	53.76	4.64	6.10	0.17
8	2.79	0.43	5.23	17.32	14.52	57.29	2.42	6.06	0.15
9	3.23	0.43	3.18	38.15	24.08	33.33	2.60	5.45	0.15
10	2.63	5.84	14.52	11.76	3.21	62.20	3.29	4.61	0.17
11	2.24	6.93	10.13	5.07	2.56	70.70	2.44	4.69	0.16
12	3.34	8.10	9.70	3.70	7.12	70.80	1.82	4.77	0.17
13	4.48	3.12	11.07	9.28	5.14	69.10	1.24	4.83	0.18
14	0.92	6.57	23.65	6.53	8.12	56.50	1.25	4.86	0.17
15	3.58	7.09	24.90	3.51	6.11	61.80	0.79	4.21	0.18
16	5.77	7.40	13.84	5.70	7.25	64.60	1.11	4.12	0.19
17	6.42	7.38	12.63	20.12	5.66	51.90	0.47	4.12	0.17
18	7.49	3.05	14.34	27.85	9.15	45.50	2.11	2.92	0.18
24	5.13	2.09	18.95	23.71	2.10	50.50	1.50	5.24	0.16
20	4.04	2.63	18.31	23.27	2.40	50.80	2.65	5.66	0.18
21	5.72	3.85	9.09	24.25	4.55	53.60	3.12	3.91	0.19
22	2.56	6.39	8.52	23.41	3.12	52.50	2.56	3.97	0.17
23	4.31	2.71	9.06	29.99	2.89	49.10	2.12	4.85	0.16
24	7.54	2.34	12.52	34.16	3.56	44.20	1.85	5.35	0.17

Table 3
Mineralogy determined by X-ray diffraction of target rock.

Constant	a	b	c	d	e
Values	0.042	17.28	−1.861	2.112	−0.796

coefficient analysis was also performed, and results are given in Table 5. As seen in Table 5, the two methods imply that the DEN, NPHI, and AC had more readily apparent relationships with brittleness. Thus, those three parameters were then included in the dataset for next simulation.

To further study the correlations coefficients between any of the well logs and the core measured brittleness data, a multiple regression analysis was also performed. Linear regression is restricted to the estimations of a typical linear model, whereas a nonlinear regression model allows variations in multiple properties simultaneously. Multiple linear regression (MLR) fits a linear equation to the learning data as follows:

$$Y = a_1X_1 + a_2X_2 + a_3X_3 + \cdots + a_nX_n + C. \quad (9)$$

This equation shows how the dependent variable Y varies with the independent variables, X_1, X_2, X_3,....., X_n, and the regression coefficients c, a_1, a_2, a_3, ..., a_n will be predicted using the data.

MLRs require basic assumptions. One assumption is that the explanatory variables must be independent, and a second is that the dependent variable must be normally distributed with a zero mean and constant variance. As a matter of fact, some methods can be effectively employed to avoid multicollinearity and thus avoid the incorporation of mutually correlated variables into the final regression equation. Here, the MLR models were calculated using the SPSS software package (Statistical Product and Service Solutions). In this study, a stepwise method was applied to determine the significant regression coefficients. In addition, the analysis of variance (ANOVA) technique was used to search for the input parameters that significantly affect the desired response. All of the obtained relationships were found to be statistically significant under Student's t-test at a 95% level of confidence. The brittleness value prediction model can be described as follows in Table 6. B_{mul} is the target shale formation brittleness derived from MLR, and DEN, SP, LLD, DTC and CNL are representative well logs. The multiple regression performance indicator is also the correlation coefficient (R^2), which the highest is approximately 0.505. The low R^2

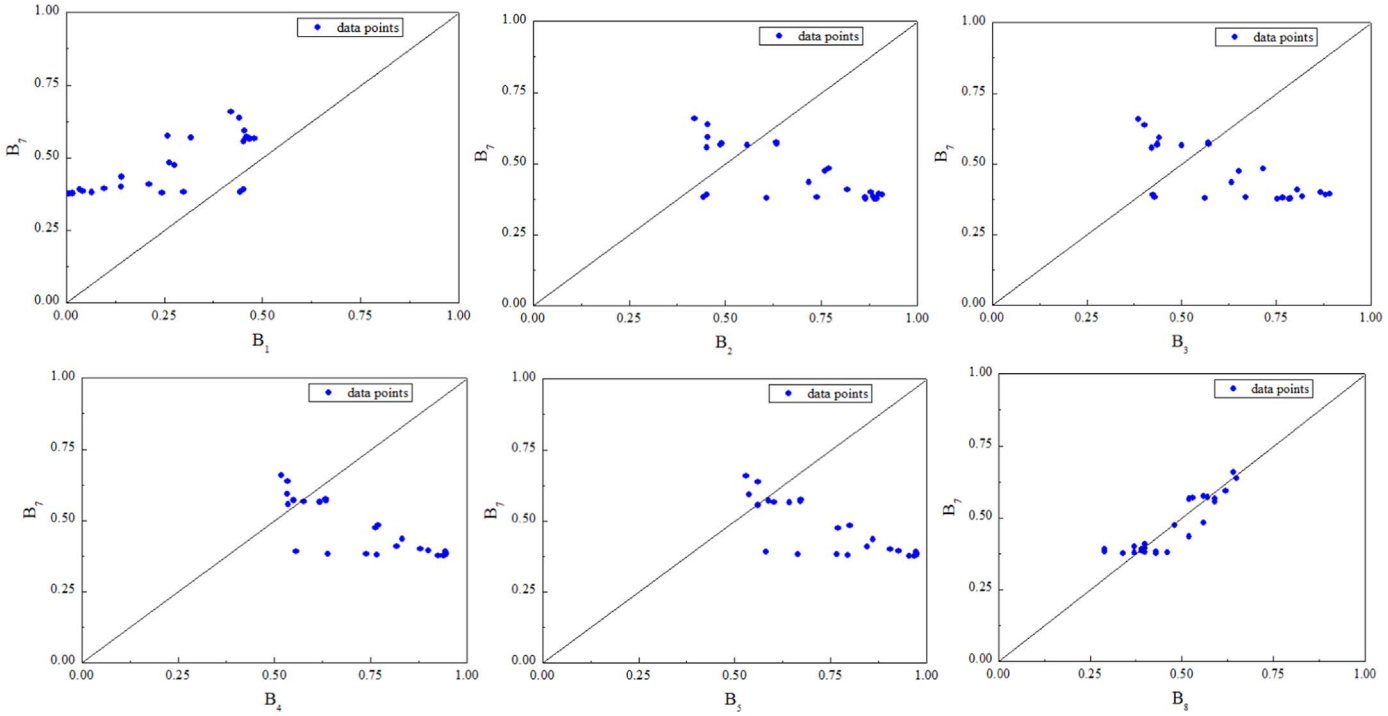

Fig. 2. Correlation between mineralogical based brittleness and elastic-based brittleness values from different brittle minerals selection (a) B_1-B_7; (b) B_2-B_7; (c) B_3-B_7; (d) B_4-B_7; (e) B_5-B_7; (f) B_8-B_7; (The blue dots represent brittleness). (For interpretation of the references to color in this figure legend, the reader is referred to the web version of this article.)

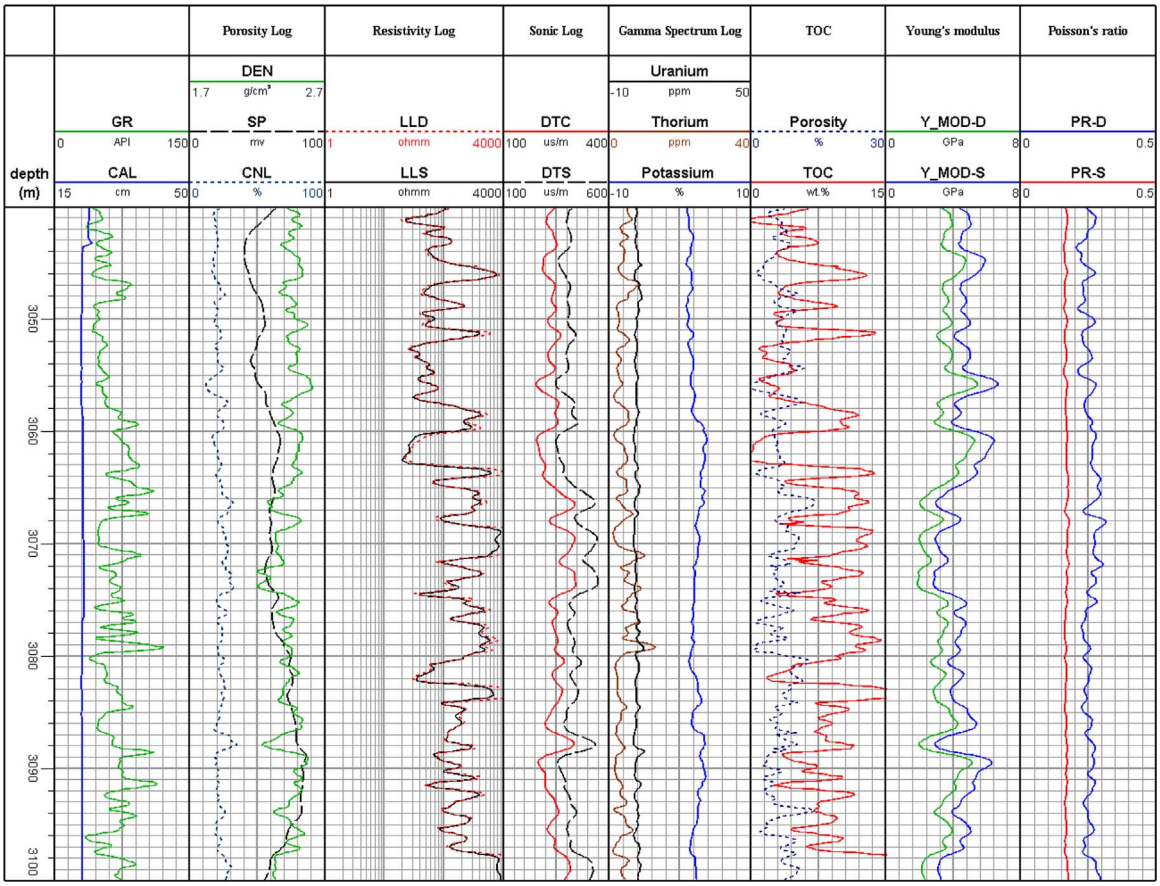

Fig. 3. Well log data and calculated elastic parameters of well H in Santanghu tight oil formation.

Table 4
Statistical values of well logs in modeling.

	Min	Max	Mean	SD
DEN	2.21	2.6	2.4377	0.07792
GR	38.71	122.99	71.39	19.09
NPHI	11.96	34.67	23.0996	3.48082
DTC	243.96	303.74	243.5667	25.49883
ILD	4470.6	9755.51	7239.9206	1362.1541
SP	48.09	83.34	67.9465	9.46704

demonstrates the inadequacy of MLR models.

4. ANN theory

In recent years, new computational intelligence techniques such as artificial neural networks, fuzzy inference systems, extreme learning machines, and support vector machines and their hybrids have been successfully employed as predictive models. Artificial neural networks (ANNs), which are based on parametric and statistical models, are the most widely used techniques in computational intelligence fields (Ma et al., 2009; Li et al., 2009). When ANNs are used to correlate non-linear systems, they can be viewed as a universal approximator (Baghban et al., 2015).

The basic processing element of an ANN is called a neuron. It receives the inputs from samples and extracts hidden functional features of a given dataset, even if the functional mappings are unknown or difficult to recognize, combines them, in general performs a nonlinear operation on the result and provides the final result. Multilayer perceptron neural networks (MLPNNs) and radial basis function neural networks (RBFNNs) are two of the most widely used neural network architectures. MLPNNs are actually the most popular neural networks in practical applications, especially when Deep Belief Networks are used to address large datasets (Hinton and Salakhutdinov, 2006). In comparison to the common three layer MLPNN, Basis Function neural networks (RBFNNs) perform much better due to their advantageously rapid training speeds and simple architectures. In addition, RBFNNs have a localized type of learning that is responsive only to a limited section of the input space.

The estimation of rock brittleness is essentially a complex classification problem that is not linearly separable task in most cases. MLPNN and RBFNN can learn from a large number of data and can be adapted to real applications with good generalization (Haykin, 2004). All of the input parameters and targets were scaled such that they fell in the range of [0,1]. The data were then divided into two datasets: training (70% of the data) and testing (30% of the data). For the neural network analyses, a software simulation written in the Matlab R2012a environment was used. As processing units, the two trained neural models constitute networks of parallel-distributed systems. However, there are still some basic distinctions between MLPNN and RBFNN in addition to their inherence constructions.

4.1. Multi-layer perception neural network (MLPNN) model

Multilayer perceptron (MLP) neural networks (Fig. 5) typically contain three types of layers: an input layer, one or more hidden layers, and an output layer. There are a given number of neurons in each layer, and the number of hidden layers and neurons greatly affect the operation of the ANN. Generally, the number of neurons in the input and output layers are determined by the data itself, whereas the number of hidden neurons varies with the specific problem. Previous studies have indicated that a single hidden layer was efficient for simulating problems and minimized the total error. More than a single layer can potentially lead to a large number of local minima and can

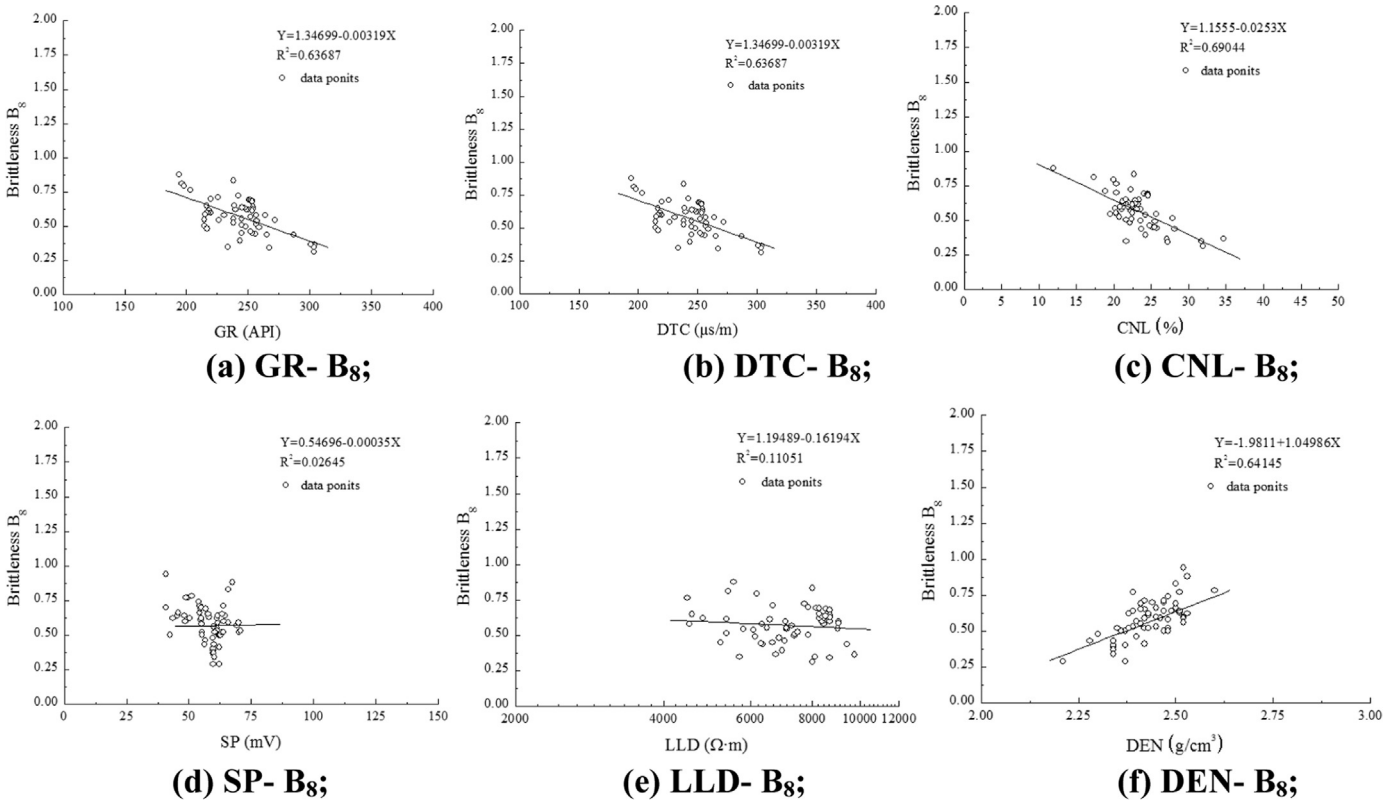

Fig. 4. Correlation of determination between B_{20} obtained from mineralogical content data of specimens and the logging data from well H. (a) GR-B_8; (b) DTC-B_8; (c) CNL-B_8; (d) SP-B_8; (e) LLD-B_8; (f) DEN-B_8; (The blank dots represent brittleness (B_8)).

Table 5
Correlation matrix of Well J1.

	B	DEN	NPHI	DTC	ILD	SP	GR
B	1						
DEN	0.641	1					
CNL	−0.69	−0.89	1				
DTC	−0.637	−0.893	0.84	1			
ILD	−0.097	−0.138	0.116	0.292	1		
SP	0.026	−0.089	0.008	0.041	−0.051	1	
GR	−0.082	−0.037	−0.032	−0.046	0.102	0.242	1

make training difficult. Thus, the impact of using more than one hidden layer was not analyzed. Several training algorithms such as gradient descent, resilient backpropagation, conjugate gradient and quasi-Newton algorithms can be used according to the specific problem. In this study, a Levenberg–Marquardt algorithm was used in the MLPNN models, the error was back-propagated through the model, and the optimal weights and biases were iteratively updated by employing the gradient descent method. The iteration stop criteria used in training the MLPNN depends on the generalization of the model, which then avoids the cases of underfitting and overfitting for the trained network.

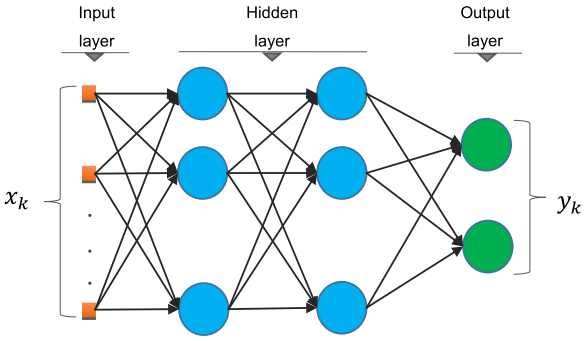

Fig. 5. Schematic representation of MLP neural network.

For underfitting, the trained model does not sufficiently learn the samples and is therefore relatively incapable of mapping the relationship from the input to output layers. For overfitting, the established network definitely gives more attention to the training samples; however, it is not as applicable for the testing samples, which then results in poor generalizations (Santos, 2013).

To investigate the performance of the trained model and validate

Table 6
Comparison of MLR models.

Inputs	MLR equations	R^2
6-log input CNL/DEN/DTC/ILD /GR/SP	$B_{mul} = -0.019CNL - 0.001DTC - 0.001GR + 0.001SP + 4.45 \times 10^{-6}LLD - 0.127DEN + 1.646$	0.505
5-log input CNL/DEN/DTC/ILD /GR	$B_{mul} = -0.019CNL - 0.001DTC - 0.001GR + 0.001SP + 4.45 \times 10^{-6}LLD + 1.253$	0.504
4-log input CNL/DEN/DTC/ILD	$B_{mul} = -0.019CNL - 0.001DTC - 0.001GR + 0.001SP + 1.265$	0.502
3-log input CNL/DEN/DTC	$B_{mul} = -0.019CNL - 0.001DTC - 0.001GR + 1.312$	0.499
2-log input CNL/DEN/	$B_{mul} = -0.019CNL - 0.001DTC + 1.254$	0.487
1-log input CNL	$B_{mul} = -0.025CNL + 1.155$	0.476

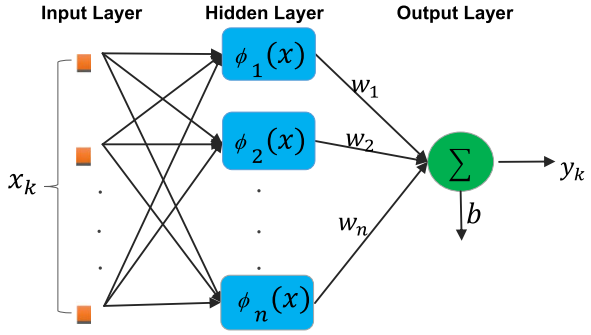

Fig. 6. Architecture of the RBF network.

the model accuracy, the minimum square error (MSE) is often used as an important metric. The equation of the MSE of the output can be written as

$$\mathrm{MSE} = \frac{1}{n\sum_{i=1}^{n}[(f(x_i) - y_i]^2}, \tag{10}$$

where f(x_i) is the actual value, y_i is the network value, and n is the number of epochs. When the MSE of a predetermined value or the maximum number of epochs have been reached, the training process stops. The trained network then can be used resimulate system outputs for inputs that have not been previously introduced (Kumar et al., 2013). A MSE of 10^{-5}, a minimum gradient of 10^{-5}, and a maximum number of epochs of 1000 were used. The training process was stopped if any of those conditions were met. The initial weights and biases of the network were assigned randomly.

4.2. Radial basis function neural network (RBFNN) model

The MLPNN and RBFNN models can be used in similar applications, but there are still some essential differences among their internal calculating structures. RBFNNs are based on an iterative approximation and localized basis functions (Huang et al., 2004). The RBFNN is a universal approximator, and it has a solid basis in conventional approximation theory (Du et al., 2006). RBFNN models are superior to MLPNN due to their simple architecture (three layers) and speed advantages (Fig. 6). In addition, they demonstrate a powerful capability to generalize the training results to unknown trials (Santos et al., 2013). Because of those features, RBFNNs are commonly substituted for MLPNNs in real applications. RBFNNs have similar structures to classical regularization networks (Girosi et al., 2490).

Fig. 6 shows the topological structure of a common RBFNN model. Typically, RBFNNs have three different layers. The first layer is comprised of input source neurons that transmit input information to the next hidden layer. Each neuron in the hidden layer corresponds to a basis function that obtains the localized output for every input sample. The second layer is a hidden layer of sufficiently large dimension that has a different purpose than that of a multilayer perceptron. The last output layer calculates the weighted sum of the outputs of the hidden neurons.

Given a training dataset D_N that consists of N input–output data samples, $D_N = \{(x_k, y_k): x_k \in R^n, y_k \in R, k = 1, 2\cdots N\}$, where x_k is the input vector of the k-th sample, and y_k is the corresponding ideal output. We assume that there are M hidden neurons in a RBFNN model. Typically, a Gaussian function is chosen as the basis function for the RBFNN, and the output of the hidden layer is

$$g(x_k) = \exp\left[-\frac{\|x_k(t) - c_i\|^2}{\sigma_i^2}\right], \tag{11}$$

where $C = \{c_1, c_2, \ldots, c_M\}$ is the center vector of the RBFNN model, and $\sigma = \{\sigma_1, \sigma_2, \ldots, \sigma_M\}$ is the width vector. The scalar output can be calculated as

$$f(x_k) = \hat{y}_k = \sum_{j=1}^{M} \omega_j g_j(x_k), \tag{12}$$

where $\omega = \{\omega_1, \omega_2, \ldots, \omega_M\}$ is the weight vector that corresponds to the M hidden neurons. The cost function to be minimized is

$$E_{mse} = \frac{1}{N}\sum_{i=1}^{N}(y_i(k) - \hat{y}_i(k))^2. \tag{13}$$

The performance of an RBFNN depends on the number and positions of the RBFNN in the hidden layer and their shape and algorithms. An evaluation was performed using an RBFNN with fixed centers selected at random that were used for rock brittleness prediction. A flowchart of the RBFNN model used for rock brittleness prediction is depicted in Fig. 6. The upper limit on the learning cycles was kept at 1000 epochs to observe the network convergence behavior, and the network goal was fixed at 10^{-5} for all of the studies.

5. Performance comparison

5.1. Performance indicators

In this paper, the performances of the MLPNN and RBFNN models are assessed using the root mean square error (RMSE) and mean absolute error (MAE) performance indicators. The MAE represents the most absolute and relative meaningful measure of the model's error, and the RMSE is a measure of the remaining measurement variance not explained by the model. The performance of the RBFNN and MLPNN models depends on the number of hidden neurons, the activation function and the stratification percentage of the training data. Thus, a number of trials were conducted to find the best combination.

$$\mathrm{MAE} = \frac{1}{n}\sum_{i=1}^{n}(f(x_i) - y_i) \tag{14}$$

$$\mathrm{RMSE} = \sqrt{\frac{\sum_{i=1}^{n}[f(x_i) - y_i]^2}{n}} \tag{15}$$

The construction of an RBFNN or MLPNN network in its most basic form involves three different layers. A number of trials were conducted initially to fix the number of neurons in the hidden layer of the RBFNN or MLPNN model according to the variation of the MSE with the number of neurons in the network configuration (Fig. 7). From the figure, it was observed that the MLPNN models were more sensitive than the RBFNN models to the number of selected neurons. For the MLPNN performance model, when the number of neurons in the hidden layer was 31, the MSE error was 0.0051, which was the minimum. Therefore, the optimum MLPNN configuration with a

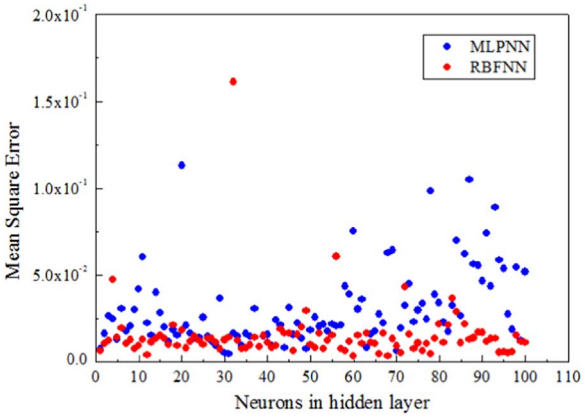

Fig. 7. Variation of MSE with the number of neurons in the hidden layer for testing algorithm.

Table 7
RBFNN model accuracy with different spread parameters.

Spread	15	25	55	105	205	300	400
MAE	0.0111	0.0344	0.2849	0.0543	0.0365	0.1315	0.0419
RMSE	0.1053	0.1855	0.5338	0.2329	0.1911	0.3626	0.2047

Levenberg–Marquardt algorithm was 6:31:1. From the figure, it can be see that the MSE reached a minimum of 0.00344 for 60 neurons, and the error increased as the number of neurons increased further. In addition, the results show that the MSE values were relatively smaller for the MLPNN model when compared to the values obtained using the same number of neurons in the MLPNN model. However, the determination of the best RBFNN configuration was more complex than in the case of the MLPNN configuration. In the testing phases of the RBFNN model, a hidden neuron calculates the Euclidean distance of the test pattern from the neuron's center and applies the RBFNN kernel function to that distance using the spread. Thus, the optimal spread in the parameters of an RBFNN model is critical to the final performance, which also requires more experimental simulation work. Table 7 shows the network error for the different spread parameters. It

Table 8
Statistical parameters of MLPNN and RBFNN model for training and validation.

Regression type	Source	MAE	RMSE	R^2
MLPNN	Training	0.0098	0.0988	0.7191
	Testing	0.0121	0.0581	0.6482
RBFNN	Training	0.0014	0.0281	0.8939
	Testing	0.0019	0.0436	0.8854

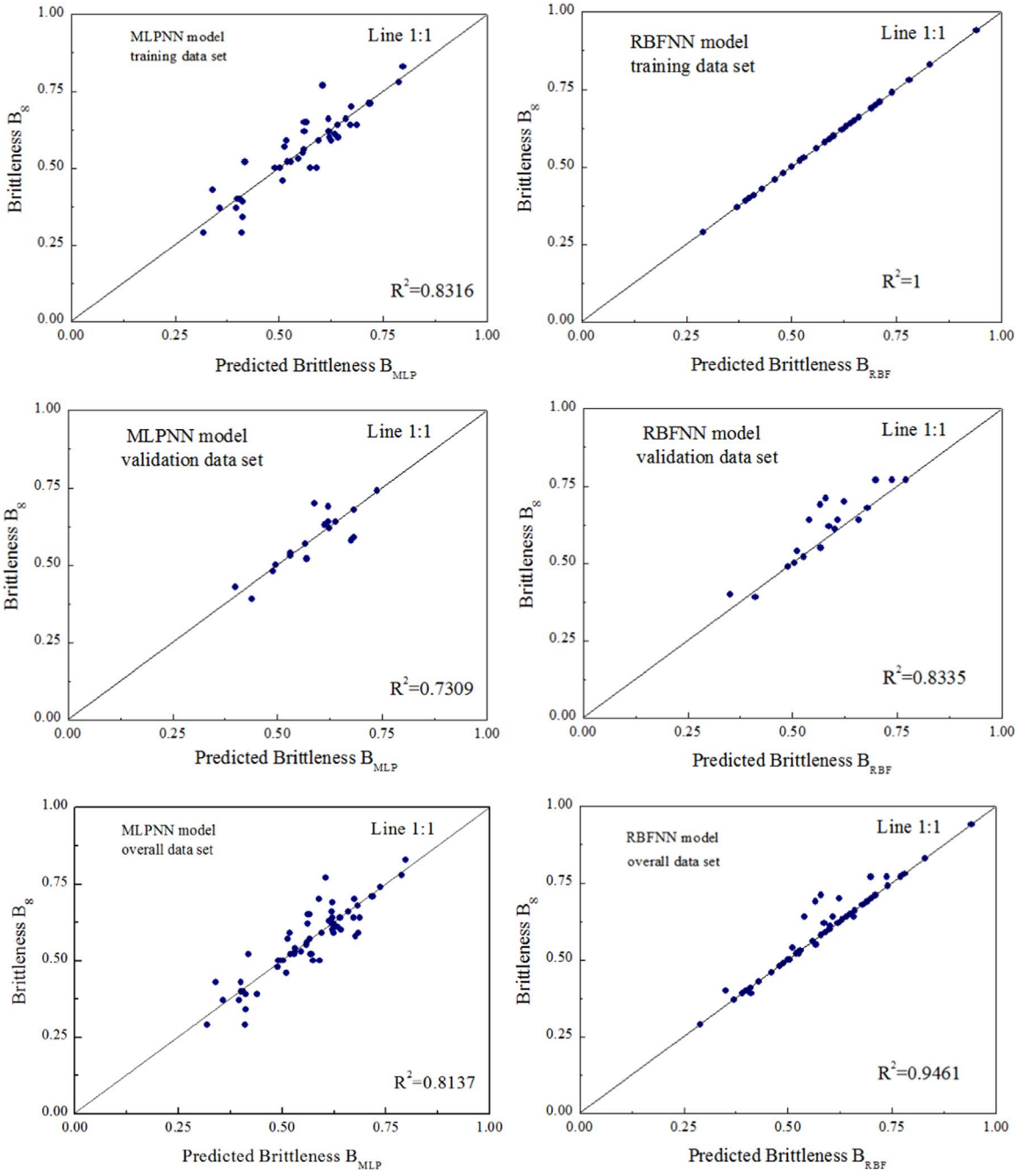

Fig. 8. Cross-correlation graphs of MLPNN and RBFNN models for training, validation and overall sets.

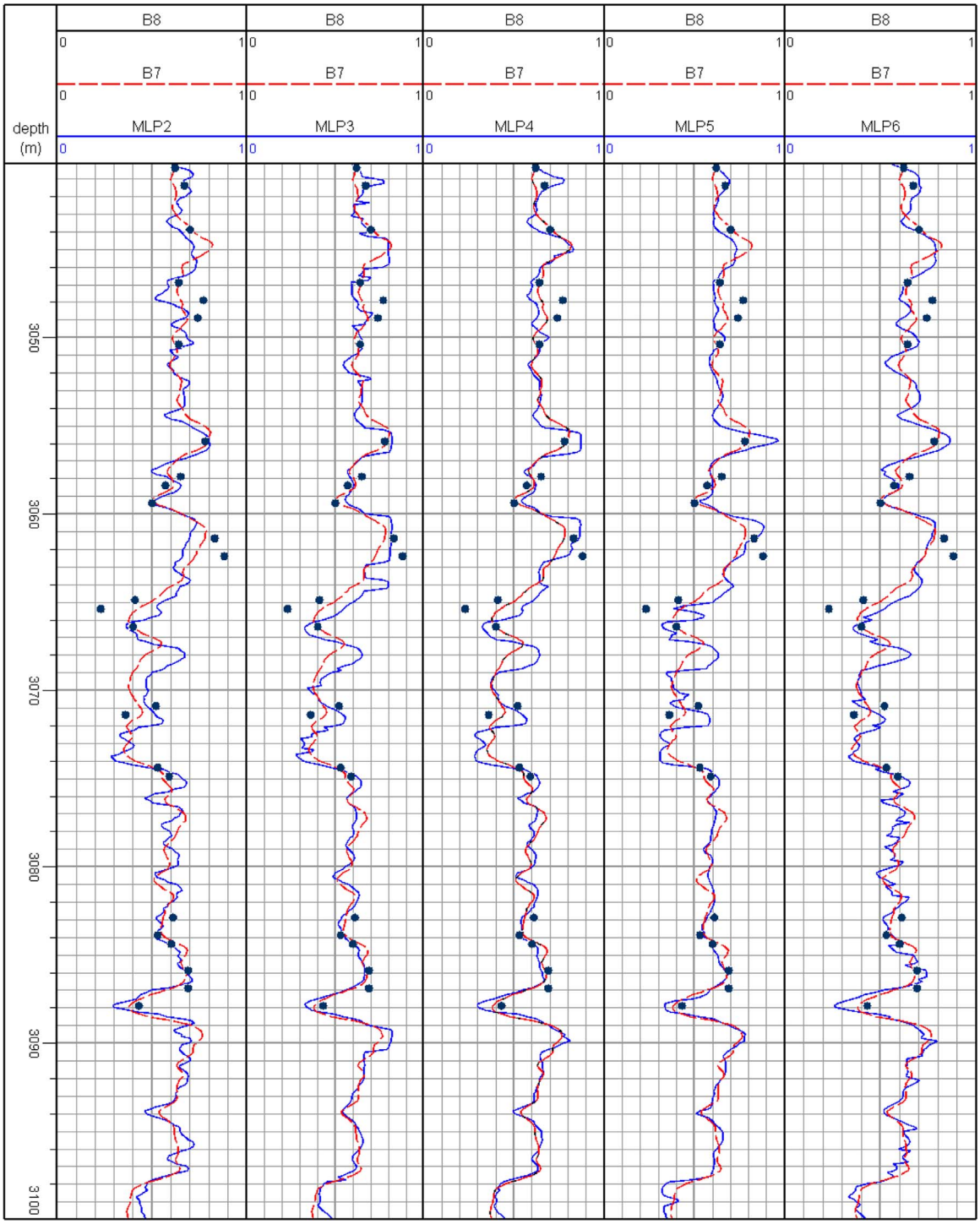

Fig. 9. MLPNN-derived brittleness prediction results with different logs as inputs, and the prediction results with elastic-based brittleness, mineralogical based brittleness in Well H. The MLP-derived results with four- and six-log inputs (MLP4 and MLP6) are consistent with the laboratory-measured brittleness results of the core samples. On the interval 3060–3070 m, it seems that the predicted results deviate mineralogical–based brittleness data (Purple dots signify mineralogical-based brittleness from core analysis, which denote as B8).

can be observed that the optimum number of spread parameters corresponded to an MAE of 0.0111 and an RMSE of 0.1053. Therefore, a spread of 15 was selected for the RBFNN construction. Hence, for the RBFNN model, the optimal network configuration was 6:60:1, with a spread parameter of 15.

To visualize the quality of the prediction, the rock brittleness predictions from the two models were compared with the measured values for the training, validation and overall datasets shown in Fig. 8. The calculated RMSE and MAE performance indicators for the RBFNN and MLPNN with the overall datasets are presented in Table 8. From the cross-correlation graphs, the performances of the models for the training and validation datasets were different. In general, the prediction performance in terms of accuracy was better for the validation set than for the training set for both models. The high performance of the models for the validation set can be considered to be an indication of the good generalization capabilities of the models. Thus, we can see that the RBFNN model yielded better results in comparison to the MLPNN models in all three phases because the RBFNN model had the lowest RMSEs in all three phases.

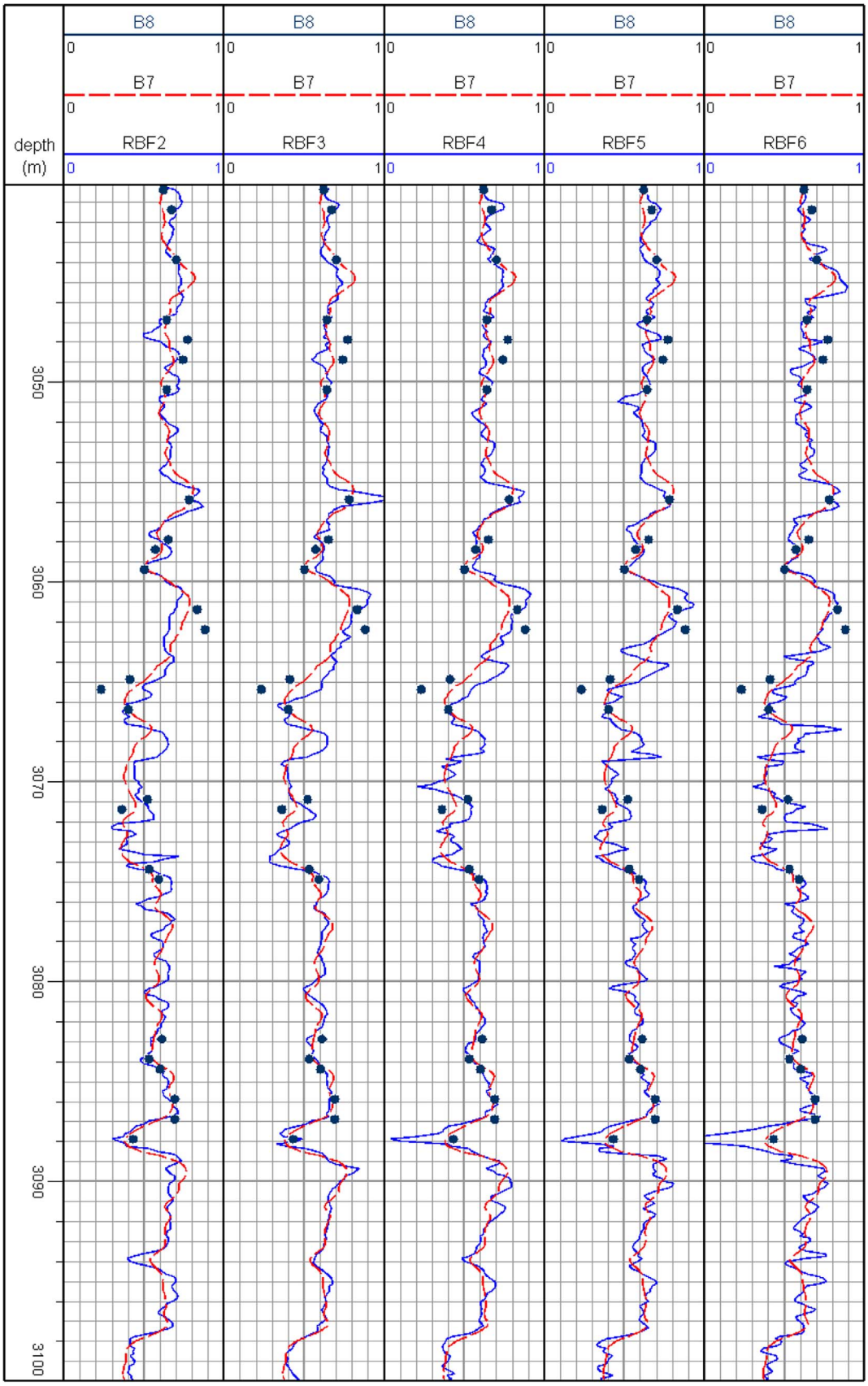

Fig. 10. RBFNN-derived brittleness prediction results with different logs as inputs, and the prediction results with elastic-based brittleness, mineralogical based brittleness in Well H. The RBF-derived results with six-log inputs (RBF6) produced best results comparing to the laboratory-measured brittleness results of the core samples. On the interval 3060–3070 m, the RBF-derived results do not perform good, either. (Purple dots signify mineralogical-based brittleness from core analysis, which denote as B8). (For interpretation of the references to color in this figure legend, the reader is referred to the web version of this article.)

Table 9
Performance comparisons for MLPNN model with different well logs as inputs.

Model types	Number of logs used as inputs	RMSE	MAE
MLPNN	6-log input CNL/DEN/DTC/ILD /GR/SP	0.0722	0.0052
	5-log input CNL/DEN/DTC/ILD /GR	0.0838	0.0071
	4-log input CNL/DEN/DTC/ILD	0.0763	0.0058
	3-log input CNL/DEN/DTC	0.085	0.0072
	2-log input CNL/DEN/	0.136	0.0185

Table 10
Performance comparisons for RBFNN model with different well logs as inputs.

Model types	Number of logs used as inputs	RMSE	MAE
RBFNN	6-log input CNL/DEN/DTC/ILD /GR/SP	0.0722	0.0052
	5-log input CNL/DEN/DTC/ILD /GR	0.0736	0.0065
	4-log input CNL/DEN/DTC/ILD	0.076	0.0058
	3-log input CNL/DEN/DTC	0.0838	0.0071
	2-log input CNL/DEN/	0.085	0.0072

5.2. Comparison of MLPNN and RBFNN approaches

The MLPNN and RBFNN computational intelligence technologies were used to estimate the brittleness of the well. The geomechanical brittleness was primarily calculated using the sonic velocity logs and density log, which was denoted as B7 and was a comparative study. Bmul represent brittleness results that calculated by MLR model with six well logs. In the process of constructing the MLPNN and RBFNN models, different inputs were chosen based on the log sensitivity ranking versus the brittleness by the coefficient relation matrix. Furthermore, the deviations between the elastic-based brittleness, mineralogical-based brittleness. MLR based brittleness and the predicted brittleness from the computational intelligence models were also calculated and are shown in Figs. 9 and 10. It can be observed that MLR model cannot produce results with high accuracy, because only limited core samples were involved in MLR model construction.

5.2.1. Comparison of MLPNN with different inputs

All of the results predicted using the MLPNN model are shown using their corresponding brittleness curves, which are denoted as MLP6 with six input logs, MLP5 with five logs, ..., and MLP2 with two logs. The results from the mineralogical-based brittleness B8, elastic-based brittleness B7 and MLPNN model yielded similar results. From the different tracks in Fig. 9 and the performance indicators in Table 9, the MAE of 0.0052 and RMSE of 0.0722 for the MLP-derived results with six-logs and the MAE of 0.0052 and RMSE of 0.0763 for the MLP-derived results with four-logs in the testing phase suggest that the predicted results have higher accuracy. Thus, we can conclude that the MLP-derived results with six and four-log inputs (MLP 6 and MLP 4) were more consistent with the laboratory-measured brittleness results of the core samples. Therefore, they were used for the fracturing perforation selection and fracturing candidate screening for this well. Conversely, the MAE of 0.0071 and RMSE of 0.0838 for the MLPNN model with five logs in the testing phase and the MSE of 0.0072 and RMSE of 0.085 for the RBFNN model with 3 logs indicate that the MLPNN method with three or five-log inputs (MLP 3 and MLP 5) also can produce acceptable results. In particular, the brittleness results were also found to be abnormal on the interval 3060–3070 m for most of the MLPNN models. Generally, these findings indicate that the MLPNN method is more effective and more accurate than a single empirical formula.

5.2.2. Comparison of RBFNN with different inputs

All the predicted results by RBFNN model were illustrated in Fig. 10, and the corresponding predicted brittleness curves were denoted as RBF6 with six logs, RBF5 with five logs, ..., and RBF2 with two logs as inputs. The predicted results and the values of the performance indicators are compared in Fig. 10 and Table 10, the MAE of 0.0052 and RMSE of 0.0722 for RBFNN with 6 well logs in the testing phase, in comparison with the MAEs and RMSEs for the RBFNN model with less than 6 well logs, indicate the better performance of RBFNN with 6 well logs for rock brittleness prediction. Thus, in this case, the prediction accuracy increased as the number of input logs increased. The results from the mineralogical based brittleness B8 and elastic-based brittleness B7 were also calculated for a comparative study with the RBFNN models. The RBFNN, B8 and B7 models yielded similar results, and, in addition, it can be observed that the deviations from the observed values of B7 predicted by the mineralogical analysis were less than those of the MLPNN models. In general, the MAE and RMSE values in the case of the RBFNN models were lower than those for the MLPNN models, and the low deviation and lower MAE and RMSE obtained by the RBFNN model proves that the prediction capability of the RBFNN model is better than that of the MLPNN models. In addition, the brittleness results were also found to be abnormal on the interval from 3060 to 3070 m, which was similar to the RBFNN models. This may be because the interval has a high mineralogical variety, and the insufficient number of training samples from this area should certainly be considered as another reason.

6. Conclusions

This paper described the application of computational intelligence technologies to rock brittleness prediction and compared the performances of the MLPNN and RBFNN models in terms of their accuracies. For this study, the conclusions can be summarized as follows.

(1) Obtaining mineralogical-based brittleness data, which are necessary for constructing the training and testing datasets, is the primary step before the construction of the network methods. According to the basin-specific and reservoir-specific characteristics, the proportion of brittle minerals needs to be adopted, and quartz, feldspar and dolomite are potentially included to calculate brittleness in some reservoirs. The results of the updated mineralogical-based brittleness using the regression method show a good consistency with the elastic-based brittleness from the in-house velocity experiments for this particular case.
(2) Establishing a relationship between rock brittleness and well log data can be very helpful for estimating rock brittleness. The results from the simple regression illustrates that there are statistical relationships between mineralogical-based brittleness, but individual well logs cannot be directly applied for brittleness prediction.
(3) Computational intelligence technologies (MLPNN and RBFNN) have been developed to detect the nonlinear and complex relationships between updated mineralogical-based brittleness and well logs. The performance of the models was checked using MSE and RMSE performance indicators. According to the performance indicators, the prediction performances of the RBFNN model were found to be better than those of the MLPNN model. The models constructed in this study can be conventionally used for initial estimates of rock brittleness and can be extended to any reservoir type.

Acknowledgments

This study was supported by the National Basic Research Program of China (No. 2015CB251206), the China National Natural Science Foundation (No. 61305075, No. 51504280), the Specialized Research Fund for the Doctoral Program of Higher Education of China (No. 20130133120014), and the Open Fund (No. G5800-I5-ZS-WX038) from Petroleum Exploration and Production Research Institute of SINOPEC. Special thanks are given to China Scholarship Council (CSC).

References

Altindag, R., 2003. Correlation of specific energy with rock brittleness concepts on rock cutting. J. S. Afr. Inst. Min. Metall. 103 (4), 163–171.

Baghban, A., Ahmadi, M.A., Hashemi Shahraki, B., 2015. Prediction carbon dioxide solubility in presence of various ionic liquids using computational intelligence approaches. J. Supercrit. Fluids 98, 50–64.

Chong K.K., Jaripatke O., Grieser W.V., Passman, A., 2010. A completions road map to shale-play development: A review of successful approaches toward shale-play stimulation in the last two decades. In: SPE 130369. International Oil and Gas Conference and Exhibition in China. Beijing, China.

Cipolla C.L., Warpinski N.R., Mayerhofer M.J., Lolon E.P., Vincent M.C., 2008. The relationship between fracture complexity, reservoir properties, and fracturetreatment design. In: SPE 115769, presented at the SPE Annual Technical Conference and Exhibition. Denver, Colorado, USA.

Huang, G.B., Zhu, Q.Y., Siew, C.K., 2004. Extreme learning machine: a new learning scheme of feedforward neural networks. Int. Jt. Conf. Neural Netw. 2, 985–990.

Hajiabdolmajid, V., Kaiser, P., 2003. Brittleness of rock and stability assessment in hard rock tunneling. Tunn. Undergr. Space Technol. 18, 35–48.

Honda, H., Sanada, Y., 1956. Hardness of coal. Fuel 35, 451–461.

Li, H., Zhang, Y.P., Zheng, H.Q., 2009. Gear fault detection and diagnosis under speedup condition based on order cepstrum and radial basis function neural network. J. Mech. Sci. Technol. 23, 2780–2789.

Hucka, V., Das, B., 1974. Brittleness determination of rocks by different methods. Int. J. Rock Mech. Min. Sci. Geomech. Abstr. 11, 389–392.

Hinton, G.E., Salakhutdinov, R.R., 2006. Reducing the dimensionality of data with neural networks. Science 313 (5786), 504–507, (28 July 2006).

Jarvie, D.M., Hill, R.J., Ruble, T.E., Pollastro, R.M., 2007. Unconventional shale-gas systems: the Mississippian Barnett shale of north-central Texas as one model for thermogenic shale-gas assessment. AAPG Bull. 91 (4), 475–499.

Jin, X.C. Shah, S.N., Truax, J.A., Roegiers, J.C., 2014a. A practical petrophysical approach for brittleness prediction from porosity and sonic logging in shale reservoirs. In: SPE 170972, presented in SPE Annual Technical Conference and Exhibition. Amsterdam, The Netherlands.

Jin, X.-C., Shah, S., Roegiers, J.-C., Zhang, B., 2014b. Fracability evaluation in shale reservoirs-an integrated petrophysics and geomechanics approach. In: SPE 168589, presented at SPE Hydraulic Fracturing Technology Conference, Society of Petroleum Engineers. The Woodlands, TX, USA

Kias, E., Maharidge, R., Hurt, R., 2015. Mechanical versus mineralogical brittleness indices across various shale plays. In: SPE 174781 presented at the SPE Annual Technical Conference and Exhibition. Houston, Texas, USA.

Lai, J., Wang, G., Huang, L., Li, W., Ran, Y., Wang, D., Zhou, Z., Chen, J., 2016. Brittleness index estimation in a tight shaly sandstone reservoir using well logs. Journal of Natural J. Nat. Gas Science & EngineeringSci. Eng. 27, 1536–1545.

Ma, C.C., Gu, X.D., Wang, Y.Y., 2009. diagnosis of power electronic system based on fault gradation and neural network group. Neurocomputing 72, 2909–2914.

Rickman R. , MullenM. , Petre J. , Grieser, W. Kundert, D., 2008. A practical use of shale petrophysics for stimulation design optimization: all shale plays are not clones of the Barnett Shale. In: SPE 115258, presented at SPE Annual Technical Conference and Exhibition. Denver, Colorado, USA.

Sondergeld C.H., Newsham K.E., Comisky J.T., Rice M.C., Rai C.S., 2010. Petrophysical considerations in evaluating and producing shale gas resources. In: SPE 131768, presented at the SPE Unconventional Gas Conference. Pittsburgh, Pennsylvania, USA.

Santos, R., Ruppb, M., Bonzi, S., Filetia, A., 2013. Comparison between multilayer feedforward neural networks and a radial basis function network to detect and locate leaks in pipelines transporting gas. Chem. Eng. Trans. 32, 1375–1380.

Vahid, H., Peter, K., 2003. Brittleness of rock and stability assessment in hard rock tunneling. Tunn. Undergr. Space Technol. 18 (1), 35–48.

Wang, D.B., Ge, H.K., Wang, X.Q., Wang, J.B., Meng, F.B., Suo, Y., Han, P., 2015. A novel experimental approach for fracability evaluation in tight-gas reservoirs. J. Nat. Gas Sci. Eng. 23, 239–249.

Wang, F.P., Gale, J.F., 2009. Screening criteria for shale-gas systems. Gulf Coast Assoc. Geol. Soc. Trans. 59, 779–793.

Zhou, H., Meng, F.Z., Zhang, C.Q., Xu, R.C., Lu, J.J., 2014. Quantitative evaluation methods of rock brittleness based on the stress strain curve. Chin. J. Rock Mech. Eng. 33 (6), 1114–1122.